RC24594 (W0806-115) June 27, 2008
Physics

IBM Research Report

Measurements of Band to Band Tunneling in Bulk Silicon as a Function of Crystal Orientation

P. M. Solomon, Leathen Shi, W. Haensch
IBM Research Division
Thomas J. Watson Research Center
P.O. Box 218
Yorktown Heights, NY 10598

Research Division
Almaden - Austin - Beijing - Cambridge - Haifa - India - T. J. Watson - Tokyo - Zurich

LIMITED DISTRIBUTION NOTICE: This report has been submitted for publication outside of IBM and will probably be copyrighted if accepted for publication. It has been issued as a Research Report for early dissemination of its contents. In view of the transfer of copyright to the outside publisher, its distribution outside of IBM prior to publication should be limited to peer communications and specific requests. After outside publication, requests should be filled only by reprints or legally obtained copies of the article (e.g., payment of royalties). Copies may be requested from IBM T. J. Watson Research Center , P. O. Box 218, Yorktown Heights, NY 10598 USA (email: reports@us.ibm.com). Some reports are available on the internet at http://domino.watson.ibm.com/library/CyberDig.nsf/home .

Measurements of Band to Band Tunneling in Bulk Silicon as a function of Crystal Orientation

P. M. Solomon, Leathen Shi, and W. Haensch

IBM, SRDC, T.J. Watson Research. Center, Yorktown Heights, NY 10598, e-mail: solomonp@us.ibm.com

Tel: (914) 945-2841, Fax: (914) 945-2141, Email: solomonp@us.ibm.com

Introduction: As technology is scaled down, band to band tunneling becomes an increasingly important source of leakage [1] as is manifested in GIDL (gate induced drain leakage currents). A transistor under conditions favorable to GIDL (high drain bias and low gate bias) is depicted in Fig. 1 where it is seen that the gate field induces tunneling in a path more or less parallel to the surface. This makes GIDL sensitive to the surface orientation of the FET. For instance in IBM's 11LP technology [2] and others, the FETs are purposely oriented in the 100 direction on a (100) wafer (45 deg. off flat) to reduce GIDL rather than in the conventional 011 direction. Easy tunneling directions are expected to lie along paths of lowest effective mass, thus one, in contradiction to the above experience, would expect 001 to be the easiest tunneling direction for silicon since four of the low transverse conduction-band effective mass (0.19) valleys are available in contrast to 011 where only two valleys are available. 111 is thus expected to be a difficult tunneling direction since the effective mass of all six valleys, projected along the tunneling direction, are large (0.41). In contrast to this, the valence split-off band in silicon (see Fig. 2 and Table 1) have low effective masses for tunneling of holes, especially in the 111 (Γ-L) direction (0.083). Systematic experimental data and reliable theoretical data are lacking, therefore we present here a timely and important experimental study of the directional dependence of band-to-band tunneling in silicon.

Experimental Methodology: We follow the experimental methodology of [3] with the difference that a heavily doped buried layer (see Fig. 3) is used in place of a heavily doped substrate and on-wafer probing is used instead of bonded samples, using a large sample (1 mm dia.) as a second substrate terminal, for both CV and IV measurements. Small samples are used (5 and 10 μm dia.) to reduce the impact of series resistance. N-P LOCOS isolated diodes were fabricated on 100, 001 and 111 substrates with eight implant conditions on four quadrants of two wafers. The conditions for Q2-5, used in the experiment are given in Table 2. TSUPREME simulations are shown in Fig.4. IV was measured with the HP 4142B SMU unit and CV was measured with the HP 4294A LCR meter, at 1MHz. Note that in this methodology [3] the lower leakage part of the CV curve is matched to a CV curve produced by an exponential doping profile ($N(x) = N_{b0} - \exp(x/\lambda)$) where N_{b0}, λ and the bandgap are the adjustable parameters. Once the profile has been derived the effective tunnel distance [4] can be calculated for any applied voltage.

Results and Discussion: IV characteristics of diodes for the three orientations and two doping conditions (2 and 5) are shown in Fig. 5. Note the strong enhancement of tunneling current for the 011 and 111 wafers. This is partly due to doping profile differences, as shown in Figs 6 and 7 where a capacitance, for a given implant condition, is larger for 111. Fig. 7 also shows the quality of the fit achieved with our fitting procedure. Given the strong field assisted diffusion evidenced in Fig. 4 it is not surprising that the profile is wafer orientation dependent. Fig. 8 shows J-V curves for the three wafers for the two sized samples. The current is substantially proportional to area, although for the 001 sample the smaller sample shows an appreciable excess current especially for the lowest doped quadrant. We believe that this is an intrinsic effect caused by the current flowing at the device periphery (see Fig. 3) in non-001 directions. The peripheral area and the current-density enhancements are large enough to account for the data. CV derived doping densities, compared to the fitting profiles are shown in Fig. 9. Note that a good match is obtained only for the lower leakage part of the CV curve used in the fitting. While the profile obviously has a lot of noise and uncertainty, the tunnel distance calculated from the profile [4] is relatively insensitive to the profile parameters (see Fig. 10) provided the capacitance at low voltages is accurately determined. Current density vs. effective tunneling distance is shown in Fig. 10. where segments of the curves are at constant voltages, each point from a separate quadrant. Note how strikingly the data are unified, as in [3], but now the 011 and 111 orientations show higher currents than 001 in agreement with GIDL experience. The effective mass (averaged over all segments) and prefactor was derived from the slope and intercept of each segment as show in Table 3. While the trend of the data shows a steeper slope for the 100 curve, the effective mass (slope of the segments) is the same (0.21) for all orientations, and the current density increase is caused by the prefactor. The relatively effective mass for the 111 direction suggests that the high projected effective mass of the conduction band valleys is somehow bypassed in the tunneling process, perhaps by the low-mass split-off valence band. The high pre-factor for the 001 ans 111 directions suggests larger number of states for tunneling or a more efficient phonon transfer process

Conclusions: We have shown an enhancement of band-to-band tunneling in the 011 and 111 directions, compared to 001, which confirms the choice made for low-power technologies of aligning FETs in the 001 direction.

References:

1. P.M. Solomon, D.J. Frank, et al, 2003 IEDM Technical Dig., P9.3.
2. http://www-01.ibm.com/chips/techlib/techlib.nsf/techdocs/C7973408D5AE2181002572E90079A79E/$file/11LP_Oct1807.pdf
3. P.M. Solomon, D.J. Frank, et al., J. Appl. Phys., v 95, n 10, May 15, 2004, p 5800-5812

4. The average tunnel distance is the average over energy of the distance between equi-energy points on the conduction and valence bands weighted by their tunneling probability. The effective tunneling distance accounts also for the effect of curvature of the bands on the WKB tunneling integral.

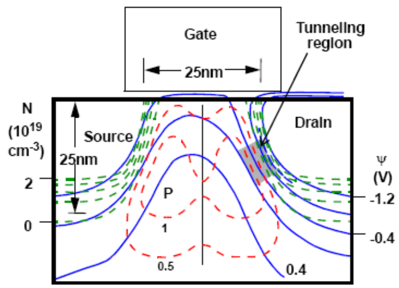

Fig. 1: This is a placeholder, awaiting an improved figure from Arvind or Jin.

Table 1: Effective masses for the split-off and light -hole valence bands, from Fig. 2

Valley.	m_h
$\Gamma_{so} \to L$	.083
$\Gamma_{so} \to X$	0.20
$\Gamma_{so} \to K$	0.13
$\Gamma \to K$	0.35

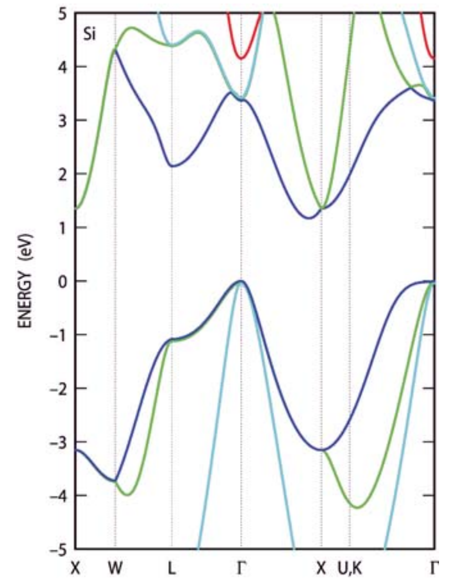

Fig. 2: Si bandstructure computed via a nearest-neighbor empirical tight binding technique using $sp^3d^5s^*$ orbitals with spin-orbit interaction included. After J.-Jancu, R. Scholz, F. Beltram and F. Bassani, Phys. Rev. B, **57**, 6493, (1998).

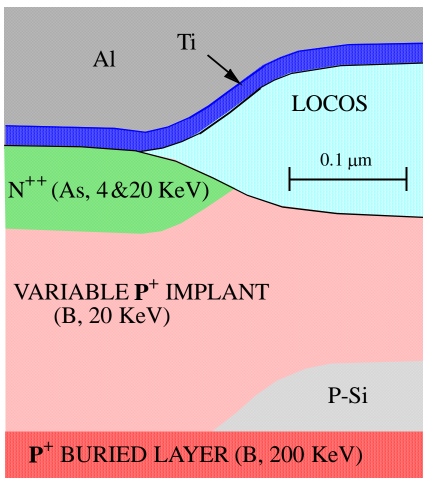

Figure 3: Schematic detail of edge of LOCOS isolated NP diode.

Table 2: Boron Dose for variable boron implants.

Quad.	B:20KeV (cm^{-2})
2	1.2E14
3	2.0E14
4	2.6E14
5	3.5E14

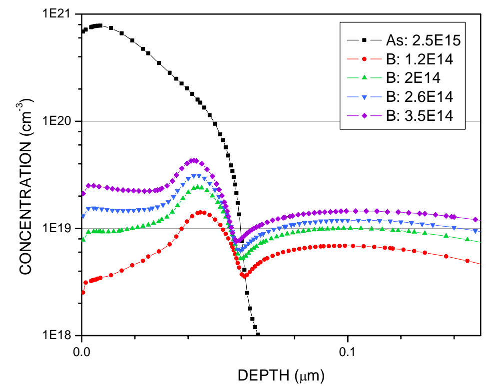

Figure 4: TSUPREME simulations of ion implattation and rapid thermal anneals, including full transient enhanced diffusion

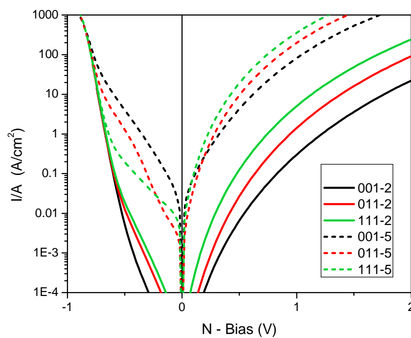

Fig. 5: Current density vs voltage for Q2 and Q5 for all crystal orientations.

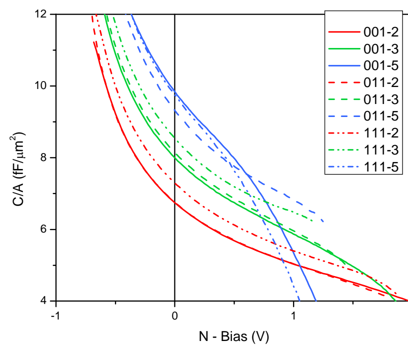

Fig. 6: CV curves, at 1MHz, for Q2, Q3 and Q5 for all crystal orientations. Downturn in curves at high bias is caused by leakage.

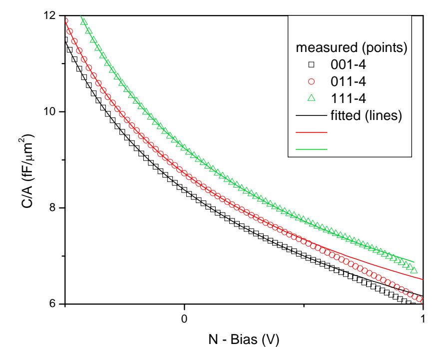

Figure 7: Detail of CV curves for Q4 showing data and exponential doping model fits.

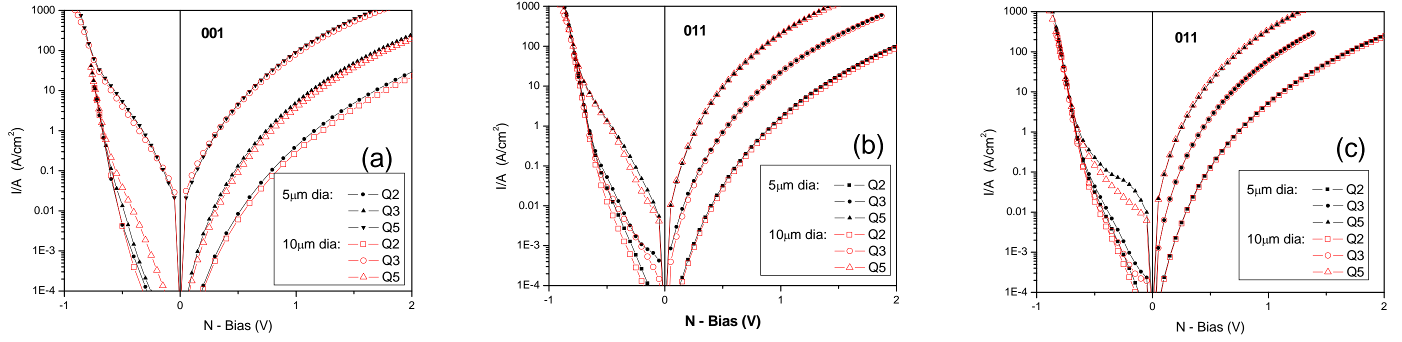

Fig. 8: Current density vs. voltage for Q2, Q3 and Q5 for 10um and 5um sample diameters. For 001 (a), 011 (b) and 111 (c) orientations

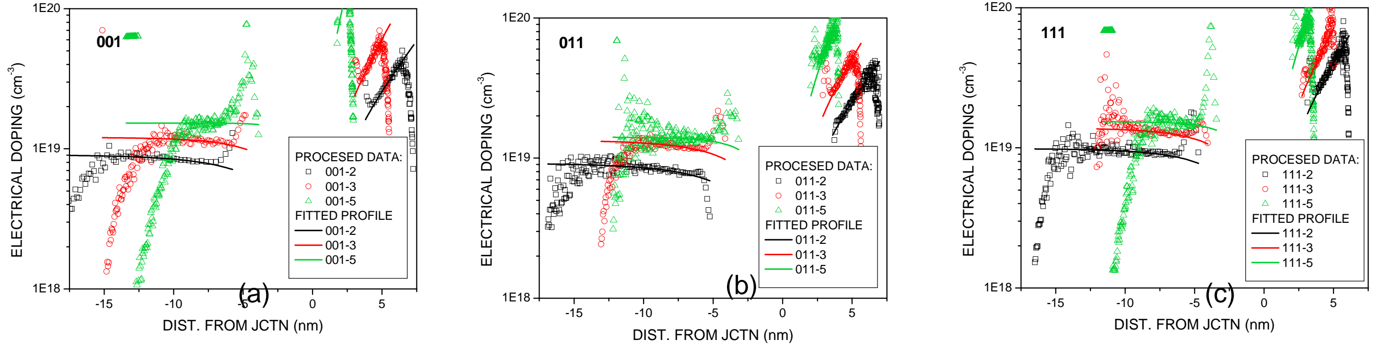

Fig. 9: Doping densities calculated from the data, compared to the fitted exponential profiles, using the ratio of left and right-hand side doping derived from the fitted profiles. Fitting parameters (Vb(V),Nb0(10^{19} cm^{-3}),λ (nm)) are (a) 001-Q2: (1.04,0.90, 3.72), Q3:(1.04,1.21,2.78), Q5:(1.12,1.53,1.06), (b) 011-Q2:(1.04,0.97,3.78), Q3:(1.02,1.34,3.17), Q5:(1.0, 1.41,1.86), and (c) 111-Q2:(1.03,0.99,3.06), Q3:(1.01,1.51,2.20), Q5:(1.02,1.54,1.68).

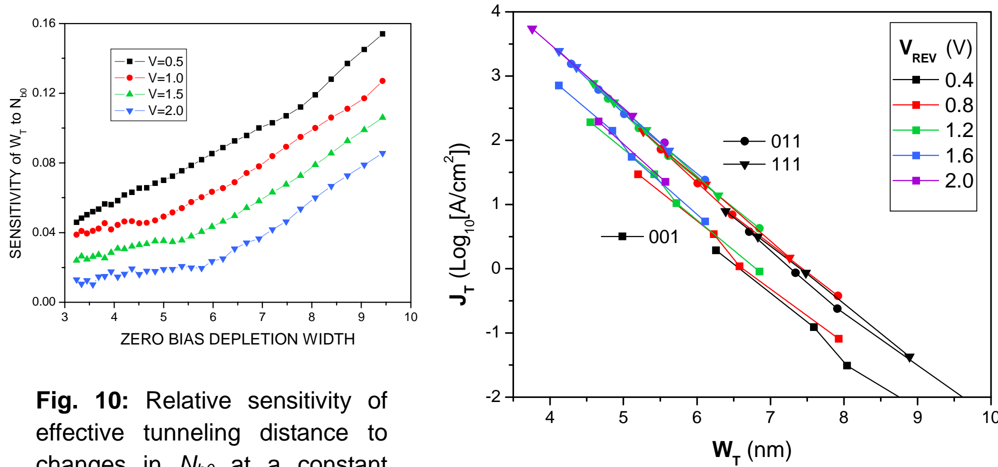

Fig. 10: Relative sensitivity of effective tunneling distance to changes in N_{b0} at a constant zero-bias depletion width.

Fig. 11: Tunneling current at a constant applied voltage vs. effective tunneling distance for 001, 011 and 111 tunneling directions.

Table 3: Efective mass (averaged over voltage segments) and current density prefactor at two applied voltages, for the 001, 001 and 111 tunneling directions, based on the data of Fig. 11.

Orien.	m_T	J_{T0} @ 0.8V (A/cm^2)	J_{T0} @ 1.6V (A/cm^2)
001	0.21	2.2e6	1.4e7
011	0.21	1.9e7	3.8e7
111	0.21	2.1e7	3.8e7